Single-target molecule detection with nonbleaching multicolor optical immunolabels

Sheldon Schultz, David R. Smith, Jack J. Mock, and David A. Schultz*

Department of Physics 0319, University of California, 9500 Gilman Drive, La Jolla, CA 92093

Communicated by Harry Suhl, University of California, San Diego, La Jolla, CA, and approved November 12, 1999 (received for review September 9, 1999)

We introduce and demonstrate the use of colloidal silver plasmon-resonant particles (PRPs) as optical reporters in typical biological assays. PRPs are ultrabright, nanosized optical scatterers, which scatter light elastically and can be prepared with a scattering peak at any color in the visible spectrum. PRPs are readily observed individually with a microscope configured for dark-field microscopy, with white-light illumination of typical power. Here we illustrate the use of PRPs, surface coated with standard ligands, as target-specific labels in an *in situ* hybridization and an immunocytology assay. We propose that PRPs can replace or complement established labels, such as those based on radioactivity, fluorescence, chemiluminescence, or enzymatic/colorimetric detection that are used routinely in biochemistry, cell biology, and medical diagnostic applications. Moreover, because PRP labels are nonbleaching and bright enough to be rapidly identified and counted, an ultrasensitive assay format based on single-target molecule detection is now practical. We also present the results of a model sandwich immunoassay for goat anti-biotin antibody, in which the number of PRP labels counted in an image constitutes the measured signal.

Robust optical reporters for diagnostic detection and/or labeling are used extensively in areas of biomedical and clinical chemistry research, for instance in immunology, microbiology, molecular biology, pharmacology, pathology, virology, or drug testing. Current methods of detection use colorimetric, fluorometric, or chemiluminescent (1) reporter molecules either as enzyme substrates or as direct labels. The measured optical signal in such assays typically results from the accumulated sum of all reporter labels present in the target region, including contributions from both specific and nonspecific binding events. Alternative optical assay formats based on detecting and counting individual binding events are possible, but have not yet been demonstrated to be feasible. Although single fluorescent molecules, upconverting phosphors (2), and the recently introduced quantum dots (3, 4) can be individually detected, such systems have very low light yield and often exhibit time-dependent blinking and irreversible photodestruction. Thus, to indicate reliably the presence of a target, a population of such labels is still required, potentially limiting both the minimum quantity of target detected and the spatial localization of the labeled region.

We introduce here a new assay platform (both probe and instrumentation) capable of individual target molecule detection that uses plasmon-resonant particles (PRPs) as optical reporters. PRPs are metallic nanoparticles, typically 40–100 nm in diameter, which scatter light elastically with remarkable efficiency because of a collective resonance of the conduction electrons in the metal (i.e., the surface plasmon resonance; ref. 5). The magnitude, peak wavelength, and spectral bandwidth of the plasmon resonance associated with a nanoparticle are dependent on the particle's size, shape, and material composition, as well as the local environment. By influencing these parameters during preparation, PRPs can be formed that have a scattering peak anywhere in the visible range of the spectrum. To illustrate this capability, as well as the ability to visualize single PRPs, a color photograph (1-sec exposure time) taken of a dark-field microscope image of a red-, a green-, and a blue-colored PRP immobilized on a silicon wafer is shown in Fig. 1*A*. The scattering spectrum corresponding to each PRP is shown in Fig. 1*B*, where the peak of each spectrum has been normalized to have the same magnitude.

For spherical PRPs, both the peak scattering wavelength and scattering efficiency increase with larger radius, providing a means for producing differently colored labels. Populations of silver spheres, for example, can be reproducibly prepared for which the peak scattering wavelength is within a few nanometers of the targeted wavelength, by adjusting the final radius of the spheres during preparation. An example of a population of PRPs with nearly homogeneous scattering characteristics is shown in the microscope image of Fig. 2*A*. For very large silver spheres, the resonance width broadens appreciably, limiting the range of usable peak wavelengths to between ≈400 and ≈500 nm. To obtain PRPs that scatter at longer wavelengths (into the red spectrum), changes in other properties, such as the material or shape, can be used.

Because PRPs are so bright, yet nanosized, they can be used as indicators for single-molecule detection; that is, the presence of a bound PRP in a field of view can indicate a single binding event. As typically prepared, PRPs have a scattering cross-section of 10^{-10} cm^2; therefore, under epi-illumination (100 W halogen) with a ×100 lens (0.9 numerical aperture), a single PRP will deliver ≈10^7 photons in 1 sec to the detector. Compared with other optical-labeling entities under the same illumination conditions, the ≈80-nm PRP scattering flux is equivalent to that from 5 million individual fluorescein molecules—1000-fold that provided from a 100-nm Fluosphere (Molecular Probes; data not shown) or $> 10^5$-fold that from typical quantum dots (3, 4).

PRPs, which have dimensions smaller than the wavelength of light, image as point sources under standard microscope optics, with a spatial extent determined by the aperture of the first objective lens. An intensity plot of the image of one of the PRPs in Fig. 2*A* is shown in Fig. 2*B*, as acquired by a charge-coupled device (CCD) camera located in the image plane of the microscope. The surface in the figure, known as the point spread function, represents a convolution of the ideal diffraction pattern of the PRP with the optics of the imaging system. The noticeable asymmetry in the ring pattern, for example, is related to both the illumination conditions and aberrations in the objective lens. A vertical section through the surface of Fig. 2*B* along a line of pixels passing through the center intensity maximum is plotted in Fig. 2*C*.

Although the width of the point spread function is much larger than the dimension of the actual corresponding PRP, owing to diffraction, the spatial coordinates of the PRP can be determined with much better accuracy by fitting the full two-dimensional image data set to an ideal point spread function.

Abbreviations: PRP, plasmon-resonant particle; PRISH, plasmon-resonant *in situ* hybridization; PRISA, plasmon-resonant immunosorbent assay; DD, double distilled; GAB, goat anti-biotin; RAG, rabbit anti-goat; CCD, charge-coupled device.

*To whom reprint requests should be addressed. E-mail: dschultz@ucsd.edu.

The publication costs of this article were defrayed in part by page charge payment. This article must therefore be hereby marked "*advertisement*" in accordance with 18 U.S.C. §1734 solely to indicate this fact.

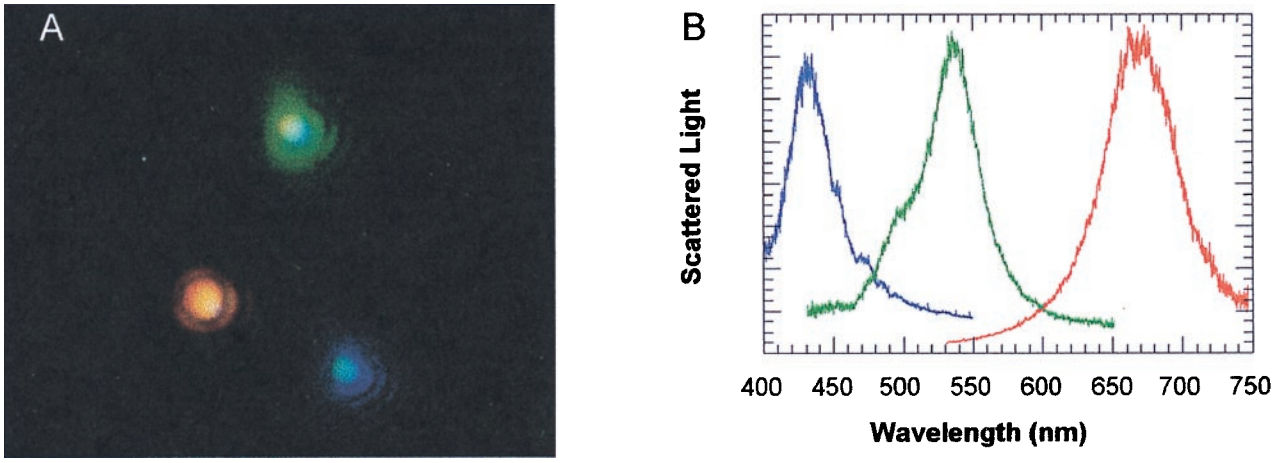

Fig. 1. (*A*) A color photograph of three PRPs illuminated with white light. The particles were chosen so that their plasmon resonance peak wavelengths would be red, green, and blue, respectively. The distance between the red and green particles is ≈4 μm. The weaker intensity of the blue PRP can be qualitatively seen by the overexposure of the film for the green and red images. (*B*) Spectral curves: the relative intensity of scattered light as a function of wavelength for the three particles shown in *A*. The two PRPs whose peak wavelengths are shifted by ≈100 nm have ≈10% overlap of intensity at the peak of their respective plasmon resonances. The full width at half height of the PRP with peak centered at ≈440 nm is ≈40 nm.

When other sources of variation are controlled, such as thermal motion or inhomogeneity in background optical index, the spatial peak of a PRP imaged by a standard CCD can be located to a precision of 10 Å. Such precision has previously been demonstrated in imaging of single fluorophores or gold nanoparticles (6). We note that, although an individual PRP can be localized with great precision, the elastic scattering from two or more PRPs of similar color cannot be separately resolved if they are located within a coherence length (roughly the wavelength of the illuminating light). Thus, for those applications requiring higher spatial resolution, PRPs of two different colors can be used.

Proteins such as antibodies can be conjugated to PRPs by techniques developed for gold colloids in light and electron microscopy, and these novel biological labels can be used in a variety of standard assays to replace less sensitive optical detection systems. Here we report on the development and use of protein-conjugated PRP reporters as labels in several exemplary biological applications.

Methods

Preparation of PRPs. For plain, uncoated PRPs (Figs. 1*A* and 2*A*), 3-nm colloidal gold nucleating cores were silver enhanced until particles of the desired size were produced. Typically, PRPs were prepared in a 20-ml vial of double-distilled (DD) water, to which 3 μl of 5-nm colloidal gold (approximate concentration, 5×10^{13} particles per ml) was added (Ted Pella, Redding, CA). The concentration of the nucleating centers used has a dramatic effect on PRP formation, not only in determining the quantity of silver required for PRP growth, but also by affecting the stability of the final colloidal solution. With a commercially available silver enhancement kit (Ted Pella), two drops of initiator (≈100 μl) was added to the solution, followed by 60 μl of silver enhancer added in 10-μl increments. The solution was continuously stirred at room temperature during the process. When the reaction was complete (after 1 or 2 min), the colloidal solution appeared a translucent yellow in transmitted light. The wavelength of the plasmon resonance for PRP samples in solution was quantitatively determined by absorbance measurements on a CARY 17D spectrophotometer. Plain PRPs were immobilized on clean glass slides or silicon wafers that were first surface treated with 0.02% alcian blue/0.5% acetic acid for 5 min, washed with DD H_2O, and air dried. The alcian blue pretreatment produces a positive charge on the slides that enhances the affinity of the negatively charged colloids for the slide surface. Silicon wafers used had a silicon dioxide layer of 100 nm and were preferred for their optical cleanliness. Samples were then rinsed in DD H_2O and dried in a compressed-air stream.

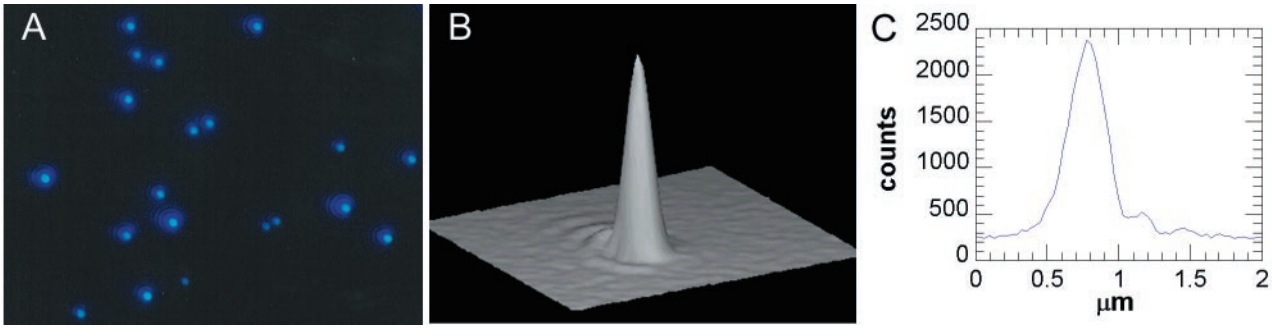

Fig. 2. (*A*) A color photograph of a collection of colloidal particles illuminated with a white light source. The area imaged is 24 × 24 μm. The particles were prepared such that their plasmon resonance peak wavelength is at ≈440 nm. (*B*) A three-dimensional–perspective CCD image of the intensity of light scattered by a single PRP. (*C*) The intensity of light measured along a line of CCD pixels passing through the maximum value of the image presented in *B*. Because the PRPs are subwavelength in size, the image of *B* is nearly that of a point source, i.e., the point spread function of the optical system. The deviations from circular symmetry are caused by asymmetry and aberrations in the objective lens.

PRP-Protein Conjugation. Conjugation of plain PRPs with proteins was carried out by procedures similar to those that have been described for conjugation of colloidal gold (ref. 7; gold colloid was purchased from BB International, Cardiff, U.K.). PRPs for the *in situ* hybridization were prepared with their resonance peak wavelength in the vicinity of 480 nm, by adjusting the amount of silver enhancer added. PRP solution (18 ml) was placed into ultraclean microcentrifuge tubes and centrifuged for 4 min at 11,750 × *g*. The supernatant was removed from the tubes, and the pellets were resuspended in 600 μl of DD H_2O. Twenty-five microliters of 100 mM sodium bicarbonate (pH 10) was added to the sample. Goat-anti-biotin [GAB (3 μg)] antibody (Pierce) was added to the PRPs, which were then incubated at room temperature with rocking. After 1 h, 100 μl of 5% BSA was added. The protein-coated PRPs were purified and separated from the excess unbound protein by centrifugation as described above. The pellet was initially resuspended in 400 μl of DD H_2O, followed by the addition of 25 μl of 10× PBS and 100 μl of 5% BSA.

For the immunoassay, 15-nm colloidal gold particles coated with rabbit anti-goat (RAG) antibody (Nanoprobes, Stony Brook, New York) were silver enhanced to produce blue PRPs. In previous work, we have found that silver enhancement of immunolabeled gold particles does not appreciably degrade the biological activity of the surface protein. Thus, preconjugated gold colloids that are themselves too small to detect visually can be silver enhanced to readily detectable PRPs. Silver enhancement can be performed before or after gold particles have been specifically bound to their target substrate.

To a 150-ml solution of 0.31% BSA, 150 μl of the 15-nm gold-RAG particles was added. While the solution was stirred, 1.75 ml of initiator was added, followed by 1.5 ml of enhancer, both added in 50-μl increments. The PRP solution was periodically spotted on slides and viewed under the dark-field microscope to monitor and control the growth of the individual PRPs. Aliquots (1 ml each) of the PRPs were spun down in ultraclean microcentrifuge tubes at 11,750 × *g* and resuspended in 20 μl of a 1:10 dilution of Tris-buffered saline/Tween (8)/0.25% BSA. The pooled fractions were used directly. The efficacy of the immunolabeled PRPs was confirmed by colorimetric tests on nitrocellulose strips spotted with various concentrations of GAB antibody.

PRP Detection and Analysis. All imaging was performed with a Nikon Optiphot microscope that had a CF Plan BD ×100, 0.9 numerical-aperture objective lens. Digital, monochrome images were acquired with a Photometrics CH200 CCD camera (KAF1400 chip) mounted on the trinocular port of the microscope head. To obtain plasmon resonance curves from individual PRPs, light was redirected via a beam splitter to an image-plane aperture (0.2-mm diameter), followed by an optical fiber centered on the optic axis. An ocular focused on the aperture was used to position PRPs into the center of the aperture. Light collected by the fiber was then transmitted into an SPEX 270M grating spectrometer, to which the Photometrics CCD camera could be mounted. The wavelength dependence of the source, optics, and CCD was removed by normalizing the spectra to the spectra obtained from a broad-band light-scattering target (Labsphere, North Sutton, New Hampshire).

***In Situ* Hybridization.** The polytene chromosome "squashes" were prepared by Seashell Technology (San Diego) as described (8). DNA encoding the white (*w*) gene genomic region was isolated from *Drosophila* chromosomal DNA by PCR amplification. Biotin-modified nucleotides were incorporated either by PCR amplification or by random priming (High Prime Biotin; Roche Molecular Biochemicals). The DNA probe was purified and concentrated by using Nuctrap columns (Stratagene) and ethanol precipitation. After hybridization with 100–300 ng of denatured-probe DNA in hybridization buffer [0.6 M sodium chloride/2× Denhardt's solution (0.02% polyvinylpyrrolidone/0.02% Ficoll/0.02% BSA)/10 mM magnesium chloride/20% dextran sulfate/100 mM sodium phosphate, pH 6.8] at 68°C for 21 h, the squashes were washed with 2× SSC at 60°C for 45 min. Before incubation with GAB PRPs for 1 h, the slides were washed with 0.5× PBS. Nonbound PRPs were removed by washing with DD H_2O.

The PRP-labeled chromosomes were stained with a 1:10,000 dilution of SYBR Green (Molecular Probes) nucleic acid gel stain solution made up in 1× PBS and placed under a coverslip. The stained and labeled chromosomes were photographed under dark-field illumination with a 75-W xenon light source. No filters were used, either in excitation or emission.

Cytological Assay. For the immunohistochemical assay, 2- to 3-μm sections of frozen chick intercostal muscle tissue were prepared as previously reported (9, 10) and transferred to either glass microscope slides for optical imaging or transmission electron microscope grids for imaging in the electron microscope. After mounting, the tissue (in all of the samples) was washed 3× for 5–10 min in PBS, then blocked for 20 min (3% normal goat serum/1% immunogold silver staining-grade gelatin/0.01% Triton X-100), and washed again for 5 min in a 1:3 dilution of PBS. After incubation with a 1:5 dilution of anti-ryanodine receptor 34C primary antibody for 1 h at room temperature, the samples were washed six times for 3–5 min each time in PBS. Next each sample was incubated with 5-nm gold colloid coated with goat anti-mouse antibody (Nanoprobes) that was diluted 1:40 in DD H_2O. The sample was then washed six times in PBS, with each wash lasting 3–5 min.

Samples on slides for optical characterization were then silver enhanced with a gelatin enhancer solution and carefully monitored, and the enhancing reaction was quenched by washing with DD H_2O when individual PRPs were visible. The gelatin enhancer solution was prepared, immediately before use, by adding 50 μl of initiator and 50 μl of enhancer to 1 ml of a 2-mg/ml gelatin solution. The gelatin solution was prepared by adding the gelatin to DD H_2O and heating to boiling temperature. The gelatin enhancer solution was placed onto the DD H_2O-rinsed chicken muscle sections for 8 min and then rinsed away.

Immunoassay. The test immunoassay was performed in the "sandwich" format. The lid of a standard 48-well dish (Corning Costar) was incubated overnight with a solution of 0.2-mg/ml biotinylated BSA (Pierce) in 100 mM sodium bicarbonate (pH 10) at room temperature. The lids, which had distinct regions indicated by raised plastic circles, were used rather than the plates themselves because the wells are too deep to allow imaging with the microscope objectives that are available. Excess, nonbound biotinylated BSA was removed by washing. Various amounts of GAB antibody (ranging from 0.06 to 10,000 pg), in 50 μl of PBS containing 0.25% BSA were incubated in the plastic wells of the lids overnight. The plastic wells were then rinsed with 0.5× PBS. In the final step, each well was incubated with 50 μl of the RAG-PRP solution, prepared as described above, for 1 h. Unbound PRPs were removed by washing with DD H_2O.

Results and Discussion

We performed three routine biological assays with antibody-coated PRPs substituted for other commonly used optical labels. All of the optical microscopic images were taken under dark-field illumination, by using a 75-W xenon arc source (see above) without any filters. In all cases, incubations or growth steps were allowed to progress just long enough that individual PRPs could still be identified, rather than allowing numerous PRPs to cluster and form aggregates. In principle, a PRP assay has single-

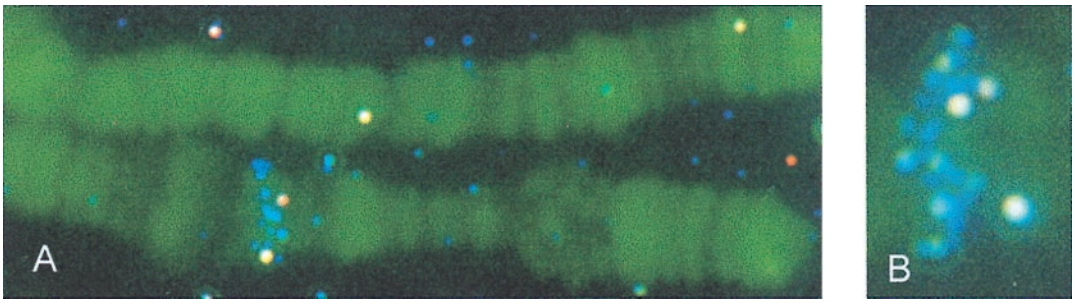

Fig. 3. Photographs of the region of the *Drosophila* X chromosome (band 3C) specifically labeled with colloidally prepared blue PRPs via the *in situ* hybridization protocol described in *Methods*. The typical distance between PRPs is ≈2 μm. The polytene chromosome is counterstained with SYBR Green. Both the SYBR Green fluorescence, and the light scattered by the PRPs are photographed simultaneously. The large number of parallel aligned copies of DNA present in the polytene chromosome provides multiple target sites for PRP hybridization, suitable for illustrative purposes, but excessive for the counting of individual PRPs for quantitative analysis. (*A*) The region of the white gene (*w*) from the tip of the X chromosome, with band 3C PRP labeled. (*B*) A close-up of the 3C band from another sample, illustrating the large density of PRPs that can be clustered yet still be readily identified as individual target site labels.

molecule sensitivity, although the relative amount of specific to nonspecific binding, the equilibrium-binding constant, and the density of target molecules set the practical limits to this sensitivity. The length of incubation time is also a factor in the signal, because each individual binding event can provide an observable change in signal. Rather than reaching equilibrium binding conditions, some signal may be sacrificed to allow for incubations that are very short compared with typical assays.

In our experiments, traditional blocking procedures adapted from protocols for assays with other labels were used without further optimization. Even so, background binding was very low (at most, several PRPs per field of view), except in some tissue areas that had high levels of background PRP binding. We believe that electrostatic interactions play a significant role in this nonspecific binding, and we are currently investigating methods for reducing this background.

The first biological assay we present here, which was performed with PRP labels, is a modification of DNA *in situ* hybridization. Nucleic acid *in situ* hybridization is a widely used biological diagnostic assay that requires sensitive reporter labels. In a typical DNA fluorescence *in situ* hybridization experiment (FISH), for example, fluorescent reporter labels are attached to nucleic acids that bind to a targeted genomic locus (11, 12). Owing to the low inherent detection sensitivity of individual fluorescent reporter molecules, amplification steps are generally needed in fluorescence *in situ* hybridization to produce a measurable signal. Such amplification techniques result in a loss of spatial information as the amplification material builds up and/or diffuses around the site being probed. In a DNA *in situ* hybridization, this loss of information limits the minimum number of bases that can be resolved between pairs of markers.

We chose to demonstrate PRP *in situ* hybridization (PRISH; Seashell Technology) by using the polytene chromosome isolated from the salivary glands of a *Drosophila* larva. In these chromosomes, ≈1000 identical DNA copies of the genome are aligned in parallel. The specific gene chosen as the target was the white gene (*w*) located near the tip of the X chromosome (band 3C; ref. 13).

The microscope image in Fig. 3 shows the tip of a SYBR Green-stained X chromosome from a *Drosophila* polytene chromosome squash after hybridization with the biotinylated *w* gene DNA probe and labeling with GAB antibody-coated PRPs. Dark-field illumination was used, with no further fluorescence filtering, so that both the chromosome and PRPs could be observed simultaneously. The typical distance between PRPs is ≈2 μm. The natural banding pattern present in the polytene chromosome allowed for visualization, identification, and confirmation of the specific site of chromosome labeling.

In Fig. 3, PRPs can be seen labeling the 3C band on the chromosome. These particles could be individually visualized after the primary hybridization. No additional amplification steps were used to enhance the signal. In fact, although the multiple, parallel aligned copies of the *Drosophila* genome available in the polytene chromosome were convenient for demonstration purposes, this density of target is not required from the standpoint of PRP labeling. Efforts are currently underway to perform the analogous experiment of labeling a human chromosome. By using two or more sets of PRPs that have different colors and surface ligands, simultaneous identification and positioning of multiple, different nucleic acid probes should be possible for DNA-mapping applications.

The second biological assay demonstrating PRP capability is a modification of immunohistochemistry in a mounted tissue sample. This assay illustrates the flexibility of the PRP-labeling system because, in samples that are resistant to penetration by entities as large as fully grown PRPs, assays can be performed with labeled colloidal gold as the probe. After gold labeling, silver enhancement can be performed, just long enough to produce visually detectable, precisely localized, individual PRPs, rather than the traditional large, dark silver masses used by light microscopists performing immunogold silver staining (7). Protein-conjugated colloidal gold particles can be obtained commercially in sizes ranging from 1 nm to hundreds of nanometers. In labeling of tissue samples for electron microscopy, for example, the smaller-sized immunogold particles (<10 nm) are preferred because of improved tissue accessibility.

To illustrate the efficacy of developing PRPs from immunogold bound to specific tissue-labeling sites in a sample, we targeted ryanodine receptors found in chicken skeletal muscle. In longitudinal sections of skeletal-muscle tissue, the ryanodine receptors are found at the triadic junctions between the sarcoplasmic reticulum and transverse tubule system. Ryanodine receptor immunoreactivity is found at the junctions of the sarcoplasmic reticulum and transverse tubule system, which are present along the *z* lines (9, 10, 14).

A color photograph of an optical dark-field image of the PRP-labeled (silver-enhanced) tissue is shown in Fig. 4*A*. The single arrow in the figure indicates a row of four bound PRPs, an intensity line plot of which is shown in Fig. 4*B*. The average spacing between PRPs, as measured from the figure, corresponds to 0.5 ± 0.05 μm, in agreement with that observed by electron microscopy.

To confirm the targeted site labeling, some of the ultrathin cryosections were prepared on transmission electron microscopic grids and labeled, as shown in the electron micrograph in Fig. 4*C*. This and other electron micrographs reveal the PRPs as

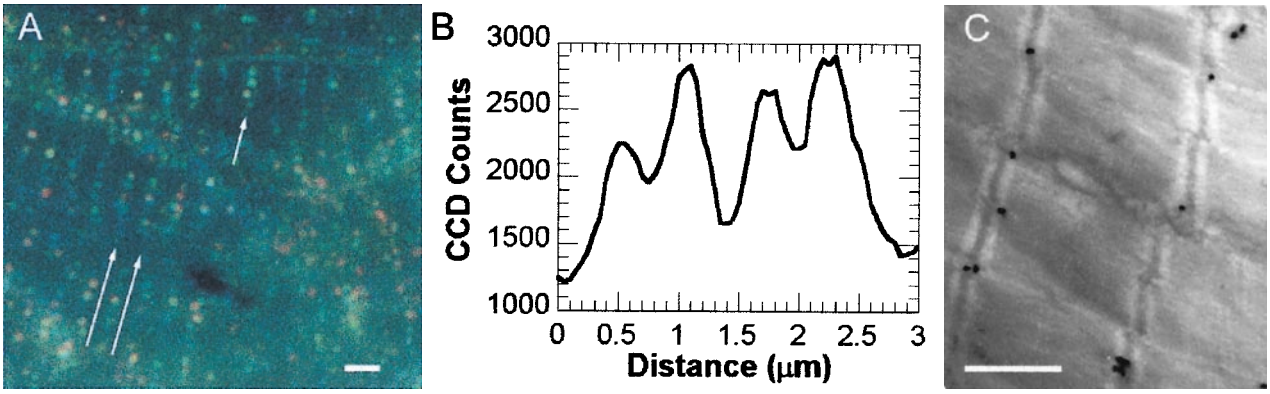

Fig. 4. (*A*) A color photograph of a chicken muscle tissue section in which the ryanodine receptors have been immunogold labeled, and then silver enhanced until individual PRPs have been formed. The optical microscope configuration and detection system is similar to that used for the data of Fig. 2. The white arrows indicate the direction of the parallel set of *z* lines located between the lines of PRPs. (Bar = 2 μm.) (*B*) An intensity (count) line scan along the direction indicated by the single arrow in *A*, demonstrating that the individual PRP image peaks are readily resolved. (*C*) A transmission electron micrograph of a tissue section similar to that used for *A*, confirming that the PRPs are found along the *z* lines in a latticelike fashion characteristic of the known spatial distribution of ryanodine receptors at the sarcoplasmic reticulum and transverse tubule system junctions. (Bar = 1 μm.)

black dots located at the triadic junctions of the sarcoplasmic reticulum and transverse tubule system. Typically, from one to five colloidal particles labeled a junction, with the junctions forming a more-or-less regular lattice of sites spaced 0.5 μm apart on average. Concentrations of initiator and silver enhancer were found, along with appropriate incubation times, which resulted in the formation of individual silver nanoparticles nucleated from the immunogold cores. If an excess of silver enhancer was used or the reaction proceeded for too long, then the nucleated silver would form large clumps of material, losing the spatial resolution.

As is well known, the electron microscope provides unparalleled spatial localization and allows visualization of (nonlabeled) features in the stained tissue. The sample preparation and observation, however, must be compatible with a vacuum environment. In the example shown above, PRPs detected by a normal light microscope allow the positions of the ryanodine receptor sites to be located optically. Moreover, the samples were successfully imaged in buffer underneath a coverslip, indicating that, *in vitro* and likely *in vivo*, real-time kinetic assays are possible with PRP labeling.

In a third example of a PRP-modified assay, we investigated the use of PRPs for quantification of target molecules in a counting-based assay in the equivalent of a "sandwich" ELISA. The ELISA, the traditional assay to determine the presence or concentration of a target molecule in a sample, typically uses labeled antibodies that bind specifically to the target. The resulting signal, for example fluorescent or colorimetric, is proportional to the sum of all reporter labels present in the sample, including those specifically bound to the target molecule as well as those from nonspecific background binding. ELISA samples are usually prepared in standard multiwell dishes and analyzed by measuring the optical density of the incubation solution (1). By contrast, in the PRP-based immunosorbent assay (PRISA; Seashell Technology), the measured signal is the numerical count of all PRPs bound to the target molecules and immobilized on the plate. Although this method can be expected to saturate at a very dense concentration of target molecules, counting individual PRPs should lead to very high sensitivity in samples with very low concentrations of target.

The results from the sandwich PRISA are shown in Fig. 5. In this test assay, a polystyrene lid from a 48-well dish, surface coated with biotinylated BSA, served as the capture substrate. Samples of GAB antibody (constituting the target), in amounts ranging from 0 (control, dark horizontal line) to 600 pg, were added into the lid wells and allowed to incubate overnight. The GAB antibody was then detected with RAG antibody-labeled PRPs. The PRPs present in the various wells, corresponding to a range of GAB antibody ("target") concentrations, were counted, and, as seen in Fig. 5, the signal covered over four orders of magnitude in concentration. A minimum detection sensitivity of ≈60 fg was achieved.

The level of sensitivity achieved in the PRISA is on a par with the most sensitive commercial assay kits. Immunosorbent assays based on PRP detection, however, have a potential advantage over alternative detection formats because the ideal assay volumes are submicroliter, sparing precious sample. Moreover, by miniaturizing the area of the capture surface, increased detection sensitivity should be realized. The individual target molecule detection provided by PRP labeling allows for this miniaturization of immunoassays, a feature important for applications such as ultra–high-throughput screening, as in combinatorial drug libraries, or DNA microarrays for functional genomics studies (15–18).

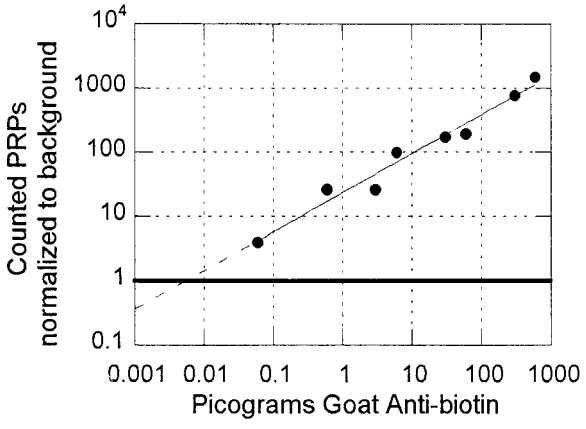

Fig. 5. Results of a PRP-based immunoassay. In this test assay, a polystyrene surface coated with biotinylated BSA served as the reaction substrate. After blocking this surface with nonbiotinylated BSA, a dilution series of GAB antibody (constituting the target), in amounts ranging from 0 (control) to 600 pg, was added and allowed to incubate overnight. After a wash step, PRPs conjugated with RAG antibodies were then incubated with the samples for 1 h, after which the samples were washed, air dried, and imaged.

The PRP-based biological assays reported here demonstrate how commonly used labels such as fluorophores can be replaced (as in the PRISA) or complemented (as in the PRISH) by PRPs. The preferred probe depends on the scattering properties of the target, as well as the quantity of material being probed. PRPs, being elastic scatterers, do not have the benefit of rejecting incident light that is scattered from the sample, as do fluorescent probes; however, in our work we have found that scattered light from PRPs can easily be discriminated from that arising from tissue or other background (e.g., Figs. 3 or 4). When the light scattered from the sample is excessive, algorithms based on recognition of the characteristic point spread function of a PRP can be used to identify the PRP and reject the background scattering.

Further studies are required to achieve the full capabilities of single-molecule detection that PRP labels provide and to demonstrate their effectiveness in the design of novel biosensors (19–22). The methodologies reported here allow for the development of many different types of assay formats. For example, one could bind PRPs to a surface via linker molecules that are susceptible to cleavage by exogenously added molecules, such as enzymes. The progressive release of the bound particles from the surface would be a measure of the amount of enzyme activity.

The results presented here, combined with the recent studies of Raman scattering from molecules surface adsorbed to PRPs (23), may result in novel biological labels and chemical sensors. In addition, the ability to localize and resolve PRPs to the precision described may also find important applications in metrology and nanotechnology (24).

We acknowledge with appreciation the preparation of the tissue section used in Fig. 4 by Professor Mark Ellisman and members of the National Center for Microscopy Imaging Research, Tom Deerinck, Victoria Edelman, and Ying Jones. We thank James Bouwer, Genalyn Rocha, and Matt Pufall at the University of California, San Diego for technical assistance and Dr. Beth Friedman of Seashell Technology (San Diego) for samples of polytene chromosomes. We thank Professors R. Doolittle, G. Feher, M. Ellisman, P. Saltman, G. Fortes, and Dr. S. L. McQuaid for critical reading of the manuscript. PRP, PRISA, and PRISH are trademarks of Seashell Technology. This research was supported by National Science Foundation Grants DMR 96–12252, 96–23949, and 97–24535; National Institutes of Health Grants 1R21HG01959–01 and 1R43HG01597; and the Richard Lounsbery Foundation.

1. Kricka, L. J., ed. (1995) *Nonisotopic Probing, Blotting, and Sequencing* (Academic, San Diego), 2nd Ed.
2. Faris, G. W., Wright, W. H., Pati, S., Schneider, L. V. & Zarling, D. A. (1996) in *OSA Trends in Optics and Photonics: Biomedical Optical Spectroscopy and Diagnostics,* eds. Sevick-Muraca, E. & Benaron, D. (Optical Soc. Am., Washington, DC), Vol. 3, pp. 225–228.
3. Warren, C. W. & Nie, S. (1998) *Science* **281,** 2016–2018.
4. Bruchez, M., Moronne, M., Gin, P., Weiss, S. & Alivisatos, A. P. (1998) *Science* **281,** 2013–2015.
5. Schultz, S., Mock, J., Smith, D. R. & Schultz, D. A. (1999) *J. Clin. Ligand Assay* **22,** 214–216.
6. Denk, W. & Webb, W. W. (1990) *Appl. Opt.* **29,** 2382–2391.
7. Hayat, M. A., ed. (1989) *Colloidal Gold: Principles, Methods and Applications* (Academic, San Diego), Vols. I, II, and III.
8. Sambrook J., Fritsch, E. G. & Maniatis, T., eds. (1989) *Molecular Cloning* (Cold Spring Harbor Lab., Plainview, NY), 2nd Ed., p B.14.
9. Lim, J. K. (1993) *Dros. Inf. Serv.* **72,** 73–77.
10. Airey, J. A., Beck, C. F., Tanksley, S. J., Deerinck, T. J., Ellisman, M. H. & Sutko, J. L. (1990) *J. Biol. Chem.* **265,** 14187–14194.
11. Sutko, J. L., Airey, J. A., Murakami, K., Takeda, M., Beck, C., Deerinck, T. & Ellisman, M. H. (1991) *J. Cell Biol.* **113,** 793–803.
12. Barch, M. J., ed. (1991) *The ACT Cytogenetics Laboratory Manual* (Raven, New York), 2nd Ed.
13. Lindsley, D. L. & Zimm, G. G., eds. (1992) *The Genome of Drosophila melanogaster* (Academic, San Diego).
14. Bloom, W. & Fawcett, D. W. (1968) *A Textbook of Histology* (Saunders, Philadelphia), 9th Ed.
15. Hieter, P. & Boguski, M. (1997) *Science* **278,** 601–602.
16. Rowen, L., Mahairas, G. & Hood, L. (1997) *Science* **278,** 605–607.
17. Fodor, S. P. A. (1997) *Science* **277,** 393.
18. Goffeau, A. (1997) *Nature (London)* **385,** 202–203.
19. Elghanian, R., Storhoff, J. J., Mucic, R. C., Letsinger, R. L. & Mirkin, C. A. (1997) *Science* **277,** 1078–1081.
20. Holtz, J. H. & Asher, S. A. (1997) *Nature (London)* **389,** 829–832.
21. Lin, V. S. Y., Motesharei, K., Dancil, K. P., Sailor, M. J. & Ghadiri, M. R. (1997) *Science* **278,** 840–843.
22. Gupta, V. K., Skaife, J. J., Dubrovsky, T. B. & Abbott, N. L. (1998) *Science* **279,** 2077–2080.
23. Nie, S. & Emory, S. R. (1997) *Science* **275,** 1102–1106.
24. Silva, T. J., Schultz, S. & Weller, D. (1994) *Appl. Phys. Lett.* **65,** 658–660.